

Article

Convective Heat Transfer of a Hybrid Nanofluid over a Nonlinearly Stretching Surface with Radiation Effect

Emad H. Aly ^{1,*}, Alin V. Roşca ^{2,†}, Natalia C. Roşca ^{3,†} and Ioan Pop ³¹ Department of Mathematics, Faculty of Education, Ain Shams University, Roxy, Cairo 11757, Egypt² Department of Statistics-Forecasts Mathematics, Faculty of Economics and Business Administration, Babeş-Bolyai University, 400084 Cluj-Napoca, Romania; alin.rosca@econ.ubbcluj.ro³ Department of Mathematics, Faculty of Mathematics and Computer Science, Babeş-Bolyai University, 400084 Cluj-Napoca, Romania; natalia@math.ubbcluj.ro (N.C.R.); popi@math.ubbcluj.ro (I.P.)

* Correspondence: emad-aly@hotmail.com

† These authors contributed equally to this work.

Abstract: The flow of the hybrid nanofluid (copper–titanium dioxide/water) over a nonlinearly stretching surface was studied with suction and radiation effect. The governing partial differential equations were then converted into non-linear ordinary differential equations by using proper similarity transformations. Therefore, these equations were solved by applying a numerical technique, namely Chebyshev pseudo spectral differentiation matrix. The results of the flow field, temperature distribution, reduced skin friction coefficient and reduced Nusselt number were deduced. It was found that the rising of the mass flux parameter slows down the velocity and, hence, decreases the temperature. Further, on enlarging the stretching parameter, the velocity and temperature increases and decreases, respectively. In addition, it was mentioned that the radiation parameter can effectively control the thermal boundary layer. Finally, the temperature decreases when the values of the temperature parameter increases.

Keywords: wall jet; hybrid nanofluid; radiation; surface temperature; numerical solution



Citation: Aly, E.H.; Roşca, A.V.; Roşca, N.C.; Pop, I. Convective Heat Transfer of a Hybrid Nanofluid over a Nonlinearly Stretching Surface with Radiation Effect. *Mathematics* **2021**, *9*, 2220. <https://doi.org/10.3390/math9182220>

Academic Editors: Francisco Ureña, Omer San and Higinio Ramos

Received: 1 July 2021

Accepted: 30 August 2021

Published: 10 September 2021

Publisher's Note: MDPI stays neutral with regard to jurisdictional claims in published maps and institutional affiliations.



Copyright: © 2021 by the authors. Licensee MDPI, Basel, Switzerland. This article is an open access article distributed under the terms and conditions of the Creative Commons Attribution (CC BY) license (<https://creativecommons.org/licenses/by/4.0/>).

1. Introduction

The analysis of flows due to stretched surface through heat transfer is considered, owing to their possible demands in several industrial procedures. The rate of stretching in a hot/cold fluids greatly depends upon the quality of the material with the desired properties. In such a process, heat transfer has an important role in controlling the cooling rate (see Fisher [1]; Tidmore and Klein [2]). Since the pioneer work done by Crane [3] on the boundary layer flow caused by stretching of elastic flat surface, a large number of researchers have investigated this problem from different points of view. The characteristics of flow and heat transfer in a boundary layer caused by a stretching/shrinking surface occurs frequently in many manufacturing processes in industry, including the extraction of polymer and rubber sheet, cooling of metallic plates, wire drawing, glassblowing, hot rolling and crystal growing, etc.

The topic of nanofluid is of scientific interest due to its many potential practical applications in biomedical, optical and electronic fields, etc. The mathematical nanofluid model was first developed by Choi [4] in 1995. Khanafer et al. [5], and Das and Tiwari [6] have examined the heat transfer performance of nanofluids inside an enclosure taking into account the solid particle dispersion. Later on, many authors discussed the effects of nanoparticles for different fluid models.

After Humnic and Humnic [7], these hybrid nanofluids are a species of fluids that contain extremely small particles of dimensions under 100 nm. They consist of two or three solid materials amalgamated with classical fluids (such as water, water ethylene glycol mixture or ethylene glycol, kerosene and engine, vegetable or paraffin oils). Many

particles can be used for the heat transfer enhancement of working fluids such as: Al₂O₃-Cu, Al₂O₃-Ag, Cu-TiO₂, Ag-TiO₂, Al₂O₃-SiO₂, etc. These fluids are utilized in tremendous heat transfer applications, such as heat pipes, micro-channel, mini channel heat sinks, plate heat exchangers, air conditioning systems, helical coil heat exchangers, etc. Comprehensive reviews on hybrid nanofluids were presented by Aly and Pop [8,9], Roşca et al. [10,11], Waini et al. [12,13], Devi and Devi [14], and in the review papers on hybrid nanofluids by Sarkar et al. [15], Akilu et al. [16], Sidik et al. [17], Sundar et al. [18], etc.

Motivated by the above-mentioned studies, this paper considers the convective heat transfer of a hybrid nanofluid over a nonlinearly stretching surface with radiation effect. In addition, the problem statement is to be described in more detail in the next section. Further, the governing equations are converted into non-linear ordinary differential equations in Section 2. Moreover, Section 3 refers to the technique of the Chebyshev pseudospectral differentiation matrix that is applied to solve the resulted equations. The present results are plotted and then discussed in Section 4. To the authors' knowledge, the present results are original and new.

2. Mathematical Model

Let us consider a hybrid Newtonian incompressible nanofluid over a flat stretching surface, where x and y are the Cartesian coordinates, which are assumed in such a manner that the x -axis runs along the surface and the y -axis is in the normal direction, the surface is laid down at $y = 0$, with the flow being at $y \geq 0$. The sheet stretches/shrinks with the velocity $u_w(x)$ and the surface temperature $T_w(x)$, while the constant ambient temperature is T_∞ . The mass flux velocity is $v = v_w(x)$ with $v(x) < 0$ for suction, while $v_w(x) > 0$ for injection, respectively, and the radiation term is q_r . The governing equations are subject to the assumption of slender boundary layer, which holds true for the case of a high Reynolds number. Under these assumptions, the governing conservation equations of mass, momentum and energy can be expressed in Cartesian coordinates (x, y) (see Kazemi et al. [19] and Devi and Devi [20]):

$$\frac{\partial u}{\partial x} + \frac{\partial v}{\partial y} = 0, \tag{1}$$

$$u \frac{\partial \bar{u}}{\partial x} + v \frac{\partial u}{\partial y} = \frac{\mu_{hnf}}{\rho_{hnf}} \frac{\partial^2 u}{\partial y^2}, \tag{2}$$

$$u \frac{\partial T}{\partial x} + v \frac{\partial T}{\partial y} = \frac{k_{hnf}}{(\rho C_p)_{hnf}} \frac{\partial^2 T}{\partial y^2} - \frac{1}{(\rho C_p)_{hnf}} \frac{\partial q_r}{\partial y}, \tag{3}$$

subject to the following boundary conditions :

$$v = v_w(x), \quad u = \left[u_w(x) = \frac{v_f}{L^{4/3}} x^{1/3} \right] \lambda, \quad T = T_w(x) + T_0 \left(\frac{x}{L} \right)^m \quad \text{at } y = 0, \tag{4}$$

$$u \rightarrow 0, \quad T \rightarrow T_\infty \quad \text{at } y \rightarrow \infty. \tag{5}$$

where u and v are the velocity components along the x - and y -axes, T is the fluid temperature of the hybrid nanofluid, T_0 is the characteristic temperature of the hybrid nanofluid, L is the characteristic length of the surface taken as the streamwise surface extent, q_r is the radiative heat flux, m describes the nonlinear boundary condition for surface temperature, where $m \neq 0$ and $m \neq 1$, and λ is the constant stretching parameter with $\lambda > 0$ and $\lambda = 0$ for stretching and static, respectively. In addition, the subscript hnf refers the hybrid nanofluid quantities, where μ_{hnf} is the effective dynamic viscosity, ρ_{hnf} is the effective density, k_{hnf} is the thermal conductivity, and $(\rho C_p)_{hnf}$ is the heat capacitance, where C_p is the specific heat at constant pressure. Further, the hybrid nanofluid quantities of Cu-Al₂O₃/water are defined as follows [20]:

$$\frac{\rho_{hmf}}{\rho_f} = (1 - \phi_2) \left[1 - \phi_1 + \phi_1 \frac{\rho_1}{\rho_f} \right] + \phi_2 \frac{\rho_2}{\rho_f}, \tag{6}$$

$$\frac{\mu_{hmf}}{\mu_f} = \frac{1}{(1 - \phi_1)^{2.5} (1 - \phi_2)^{2.5}}, \tag{7}$$

$$\frac{(\rho C_p)_{hmf}}{(\rho C_p)_f} = (1 - \phi_2) \left[1 - \phi_1 + \phi_1 \frac{(\rho C_p)_1}{(\rho C_p)_f} \right] + \phi_2 \frac{(\rho C_p)_2}{(\rho C_p)_f}, \tag{8}$$

$$\frac{k_{hmf}}{k_f} = \frac{k_2 + 2k_{bf} + 2\phi_2(k_2 - k_f)}{k_2 + 2k_{bf} - \phi_2(k_2 - k_f)}, \text{ where} \tag{9}$$

$$\frac{k_{bf}}{k_f} = \frac{k_1 + 2k_f + 2\phi_1(k_1 - k_f)}{k_1 + 2k_f - \phi_1(k_1 - k_f)}.$$

These correlations are based on physical assumptions and are in agreement with the conservation of mass and energy. Here, ϕ_1 and ϕ_2 are the hybrid nanoparticle volume fractions for Al_2O_3 and Cu, respectively, where $\phi_1 = \phi_2 = 0$ correspond to a regular fluid. Further, the subscripts $()_w, ()_1, ()_2$ and $()_f$ refer to the wall, physical quantities of Al_2O_3 , Cu and fluid (water), respectively, as given in Table 1.

Table 1. Thermophysical properties of the water and nanoparticles.

Physical Properties	Nanoparticles		
	Base Fluid Water	Al_2O_3	Cu
ρ (kg m ⁻³)	997.1	3970	8933
C_p (J kg ⁻¹ K ⁻¹)	4179	765	385
k (W m ⁻¹ K ⁻¹)	0.613	40	401

Regarding the approximation of Rosseland for radiation, the radiative heat flux is simplified as follows (see [21,22]):

$$q_r = -\frac{4\sigma^*}{3k^*} \frac{\partial T^4}{\partial y}, \tag{10}$$

where σ^* is the Stefan–Boltzmann constant and k^* is the mean absorption coefficient. Now, by expanding T^4 using a Taylor series about T_∞ and neglecting higher-order terms, T^4 is expanded about T_∞ to obtain $T^4 \cong 4T_\infty^3 T - 3T_\infty^4$. By substituting the last expression in Equation (10) and then in Equation (3), the energy equation takes the following form:

$$u \frac{\partial T}{\partial x} + v \frac{\partial T}{\partial y} = \frac{1}{(\rho C_p)_{hmf}} \left(k_{hmf} + \frac{16\sigma^* T_\infty^3}{3k^*} \right) \frac{\partial^2 T}{\partial y^2}. \tag{11}$$

According to Kazemi et al. [19], we introduce the following dimensionless variables:

$$u = \frac{\nu_f}{L^{4/3}} x^{1/3} f'(\eta), \quad v = -\frac{1}{3} \frac{\nu_f}{L^{2/3}} x^{-1/3} [2f(\eta) - \eta f'(\eta)], \quad \theta(\eta) = \frac{T - T_\infty}{T_w - T_\infty}, \quad \eta = y \frac{x^{-1/3}}{L^{2/3}}. \tag{12}$$

Thus,

$$v_w = -\frac{1}{3} \frac{\nu_f}{L^{2/3}} x^{-1/3} S, \tag{13}$$

where prime denotes differentiation with respect to η , and S is the constant mass flux parameter with $S > 0$ and $S < 0$ for suction and injection flow, respectively. Substituting

the similarity variables (12) into Equations (2) and (11), it is found that they are reduced to the following ordinary (similarity) differential equations:

$$3 \frac{\mu_{hmf}/\mu_f}{\rho_{hmf}/\rho_f} f''' + 2ff'' - f'^2 = 0, \tag{14}$$

$$\frac{3}{Pr(\rho C_p)_{hmf}/(\rho C_p)_f} \left(\frac{k_{hmf}}{k_f} + \frac{4}{3}R \right) \theta'' + 2f\theta' - mf'\theta = 0, \tag{15}$$

and the boundary conditions (4) become the following:

$$f(0) = S, \quad f'(0) = \lambda, \quad \theta(0) = 1, \tag{16}$$

$$f'(\eta) \rightarrow 0, \quad \theta(\eta) \rightarrow 0 \quad \text{as } \eta \rightarrow \infty, \tag{17}$$

where $Pr = (\rho C_p)_f/k_f$ is the Prandtl number and $R = 4\sigma^* T_\infty^3/k^*k_f$ is the radiation parameter. The physical quantities of interest are the skin friction coefficient C_f and the local Nusselt number Nu_x , which are defined as follows:

$$C_f = \frac{\mu_{hmf}}{\rho_f u_w^2} \left(\frac{\partial u}{\partial y} \right)_{y=0}, \quad Nu_x = -\frac{xk_{hmf}}{k_f(T_w - T_\infty)} \left(\frac{\partial T}{\partial y} \right)_{y=0} + x(q_r)_{y=0}. \tag{18}$$

Using Equations (12) and (18) results in the following:

$$Sr = Re_x^{1/2} C_f = \frac{\mu_{hmf}}{\mu_f} f''(0), \quad Nur = Re_x^{-1/2} Nu_x = -\left(\frac{k_{hmf}}{k_f} + \frac{4}{3}R \right) \theta'(0), \tag{19}$$

where $Re_x = u_w(x)x/v_f$ is the local Reynolds number, and Sr and Nur are the reduced skin friction coefficient and reduced Nusselt number, respectively.

3. Numerical Approach

The numerical technique of the Chebyshev pseudospectral differentiation matrix (ChPDM) is applied to solve Equations (14) and (15) subject to the boundary conditions (16). The works of Aly et al. [23], Guedda et al. [24], Aly and Vajravelu [25], Aly and Sayed [26], Aly and Pop [27] contain more details about this approach. In particular, one supposes that the problem’s domain is $[0, \eta_\infty]$, where η_∞ is the boundary-layer edge. Then, the following mapping

$$\gamma = \frac{2\eta}{\eta_\infty} - 1 \tag{20}$$

transfers the investigated domain to $[-1, 1]$ (the Chebyshev one). It should be noted that, in this interval, the associated collocation points are given by the following:

$$\gamma_j = \cos\left(\frac{\pi}{N} j\right), \quad j = 0, 1, \dots, N. \tag{21}$$

Hence, the k th derivative of any function, say $\mathbf{F}(\gamma)$, at these collocation points is approximated as the following:

$$\mathbf{F}^{(k)} = D^{(k)}\mathbf{F}, \tag{22}$$

where $D^{(k)}\mathbf{F}$ is the Chebyshev pseudospectral approximation of $\mathbf{F}^{(k)}$ and $\mathbf{F} = [F(\gamma_0), F(\gamma_1), \dots, F(\gamma_N)]^T$ with $\mathbf{F}^{(k)} = [F^{(k)}(\gamma_0), F^{(k)}(\gamma_1), \dots, F^{(k)}(\gamma_N)]^T$. Further, the entries of the matrix $D^{(k)}$ are given by the following:

$$d_{i,j}^{(k)} = \frac{2\Omega_j}{N} \sum_{r=k}^N \sum_{\substack{\ell=0 \\ (\ell+r-k)\text{even}}}^{r-k} \Omega_r b_{\ell,r}^k (-1)^{\lfloor \frac{rj+\ell i}{N} \rfloor} \gamma_{rj-N\lfloor \frac{rj}{N} \rfloor} \gamma_{ni-N\lfloor \frac{ni}{N} \rfloor}. \tag{23}$$

Here, $\Omega_j = 1$, except for $\Omega_0 = \Omega_N = \frac{1}{2}$ and

$$b_{\ell,r}^k = \frac{2^k r}{(k-1)! c_\ell} \frac{(\chi - \ell + k - 1)! (\chi + k - 1)!}{(\chi)! (\chi - \ell)!}, \tag{24}$$

where $2\chi = r + \ell - k$ and $c_0 = 2, c_j = 1, j \geq 1$. Therefore, on applying the ChPDM approach, derivatives of the functions $f(\gamma)$ and $\theta(\gamma)$ at the points γ_i are taken as follows:

$$f^{(k)}(\gamma_j) = \sum_{i=0}^N d_{i,j}^{(k)} f(\gamma_j), \theta^{(k)}(\gamma_j) = \sum_{i=0}^N d_{i,j}^{(k)} \theta(\gamma_j), k = 1, 2, 3, i = 1, 2, \dots, N. \tag{25}$$

Therefore, Equations (14)–(16) become the following:

$$3 \frac{\mu_{hnf} / \mu_f}{\rho_{hnf} / \rho_f} \sum_{j=0}^N d_{i,j}^{(3)} f(\gamma_j) + \frac{\eta_\infty}{2} \left(2f(\gamma_i) \sum_{j=0}^N d_{i,j}^{(2)} f(\gamma_j) - \left(\sum_{j=0}^N d_{i,j}^{(1)} f(\gamma_j) \right)^2 \right) = 0, \tag{26}$$

$$\frac{3 \left(\frac{k_{hnf}}{k_f} + \frac{4}{3} R \right)}{Pr(\rho C_p)_{hnf} / (\rho C_p)_f} \sum_{j=0}^N d_{i,j}^{(2)} \theta(\gamma_j) + \frac{\eta_\infty}{2} \left(2f(\gamma_j) \sum_{j=0}^N d_{i,j}^{(2)} \theta(\gamma_j) - m\theta(\gamma_j) \sum_{j=0}^N d_{i,j}^{(1)} f(\gamma_j) \right) = 0, \tag{27}$$

$$f(\gamma_N) = S, \sum_{j=0}^N d_{N,j}^{(1)} f(z_j) = \frac{\eta_\infty}{2}, \theta(\gamma_N) = 1,$$

$$\sum_{j=0}^N d_{0,j}^{(1)} f(\gamma_j) = 0, \theta(\gamma_0) = 0, \tag{28}$$

Finally, it should be mentioned that the resulting nonlinear Equations (26) and (27) with the boundary conditions (28) contain $2N - 1$ equations for the unknowns $f(\gamma_j), j = 1, 2, \dots, N$ and $\theta(\gamma_j), j = 1, 2, \dots, N - 1$. These equations are solved using the Newton method by executing them in MATHEMATICA 9TM software and running on a PC.

4. Results and Discussion

In this research, the Prandtl number Pr of the base fluid (water) is fixed at 6.2. Firstly, the nanofluid Al_2O_3/H_2O is produced by adding the Al_2O_3 nanoparticles with a fixed volume fraction $\phi_{Al_2O_3} = 0.1$. Then, the hybrid nanofluid $Cu-Al_2O_3$ /water is made by mixing Cu -nanoparticles with $0 < \phi_2 \leq 0.1$ to this nanofluid. Influences of the various physical parameters on the velocity and temperature for the resulted hybrid nanofluid are presented in the remaining of the current section.

Impacts of S on the velocity profiles $f'(\eta)$ and temperature distributions $\theta(\eta)$ are presented in Figures 1 and 2, respectively. It can be seen from Figure 1 that the rising of S leads to slowing down the $Cu-Al_2O_3$ /water velocity. This leads to decreasing the hybrid nanofluid temperature, as seen in Figure 2. Effects of the sheet parameter λ on $f'(\eta)$ and $\theta(\eta)$ are illustrated in Figures 3 and 4, respectively. As shown in these figures, as λ enlarges, the velocity and temperature increases and decreases, respectively.

Figure 5 presents the temperature distributions $\theta(\eta)$ for various values of the thermal radiation (R). This figure shows that enlarging R increases $\theta(\eta)$. It is known that the radiation parameter measures the relation between the conduction heat transfer and thermal radiation transfer. Hence, the increasing of R is indicative of a larger amount of radiative heat energy being poured into the system, which causes a rise in the temperature. Regarding this, the radiation can control the thermal boundary layers.

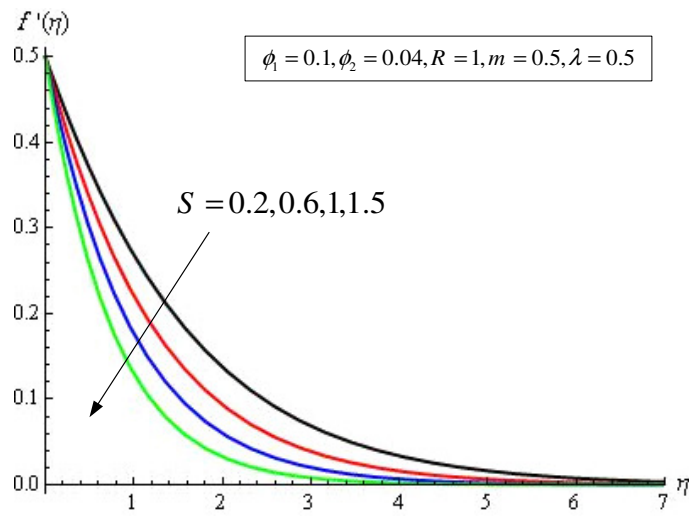


Figure 1. Velocity profiles $f'(\eta)$ for various values of S .

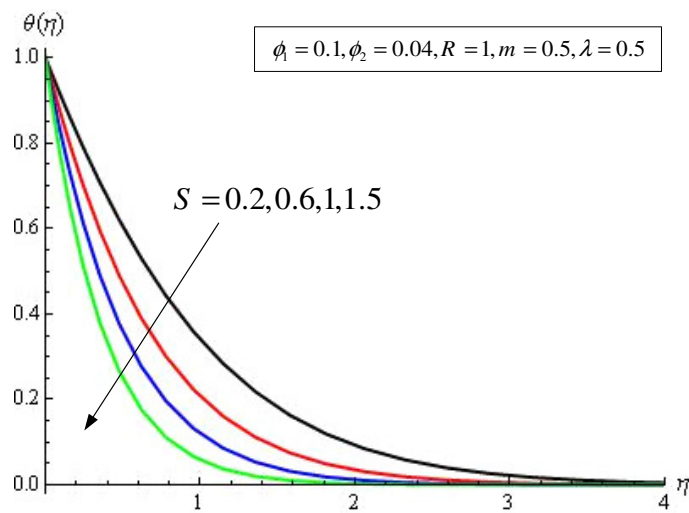


Figure 2. Temperature distributions of the hybrid nanofluid for various values of S .

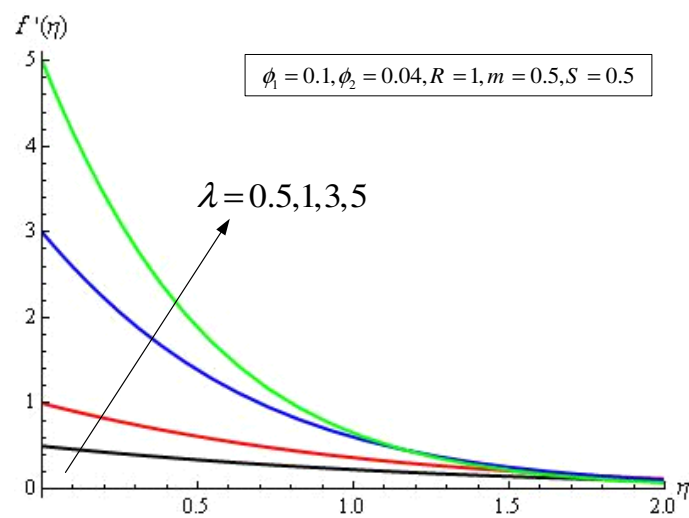


Figure 3. Velocity profiles $f'(\eta)$ for various values of λ .

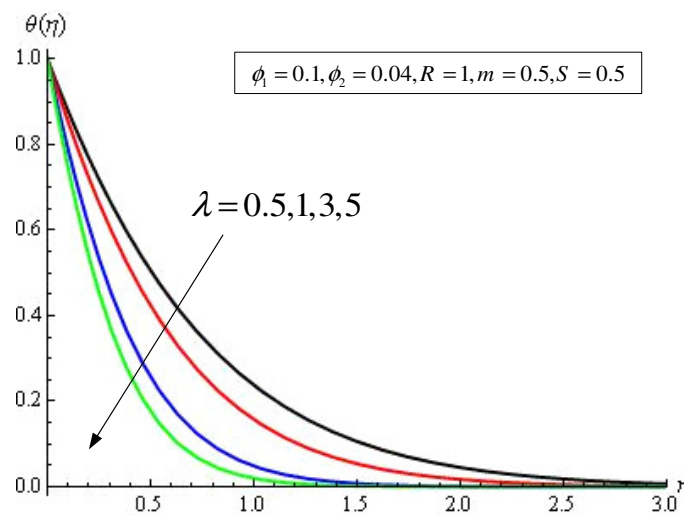


Figure 4. Effects of λ on the temperature distributions of the hybrid nanofluid.

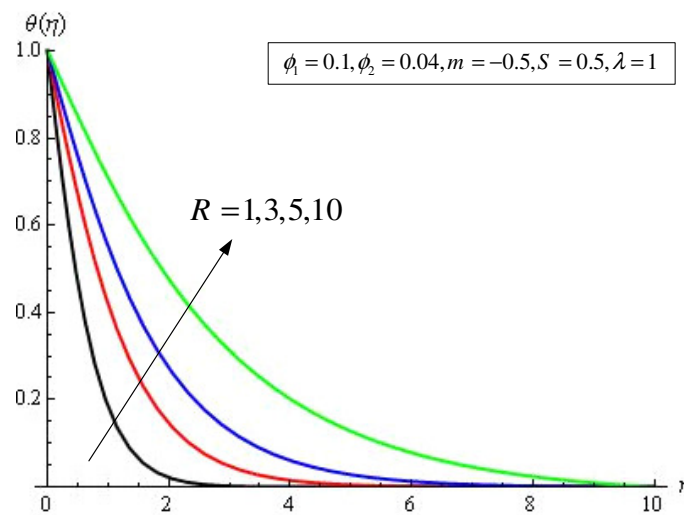


Figure 5. Influence of the thermal radiation parameter R on the temperature distributions.

Figure 6 indicates that an increase in the surface temperature parameter m decreases the dimensionless temperature. Influences of the solid volume fraction ϕ_2 on the temperature distributions are plotted in Figure 7. As seen in this figure, $\theta(\eta)$ increases as the Cu-nanoparticles concentration increases. This is because the rising of the hybrid nanofluid concentration generates more kinetic energy in the system. This means that ϕ_2 plays an important role in the variation of the temperature. Effects of the reduced Nusselt number (Nur) as a function of η for various values of R , m , S and λ are shown in Figure 8. From these figures, it can be seen that Nur increases by enlarging all of these parameters. The future research trends of this work may be stated as including the magnetic field strength, velocity slip parameters, effects of another hybrid nanofluid and variation of the radiation parameter.

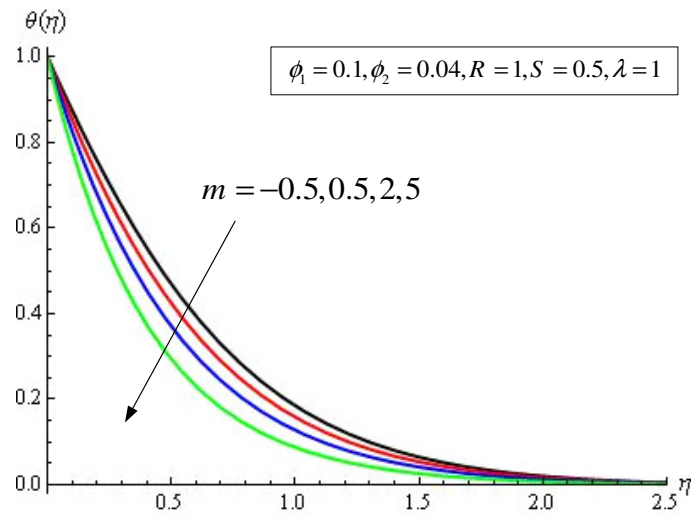


Figure 6. Impact of m on the temperature distributions of the hybrid nanofluid.

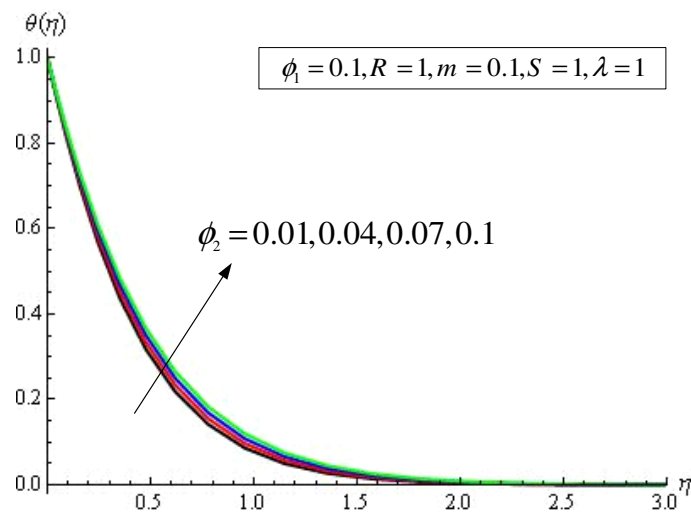


Figure 7. Impact of the Cu-nanoparticle volume fraction (ϕ_2) on the temperature distributions.

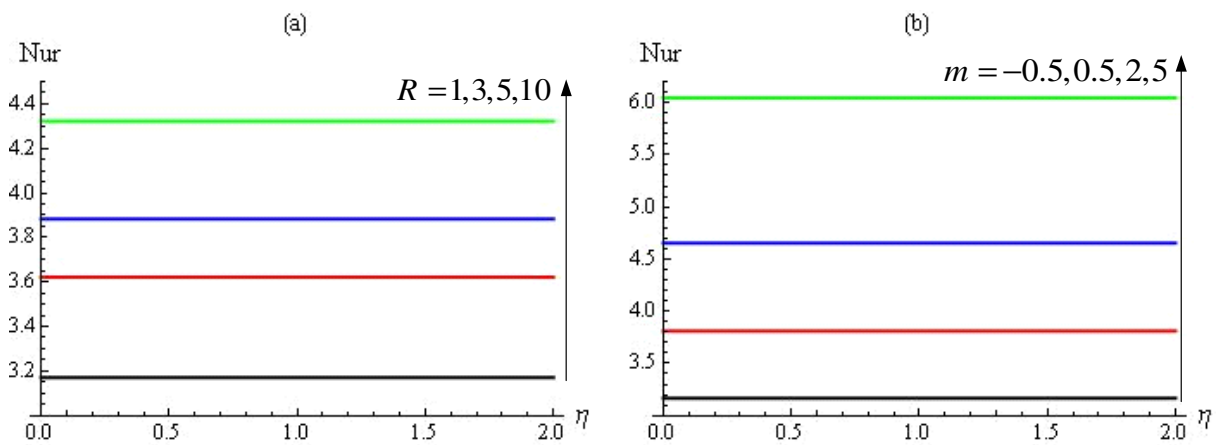


Figure 8. Cont.

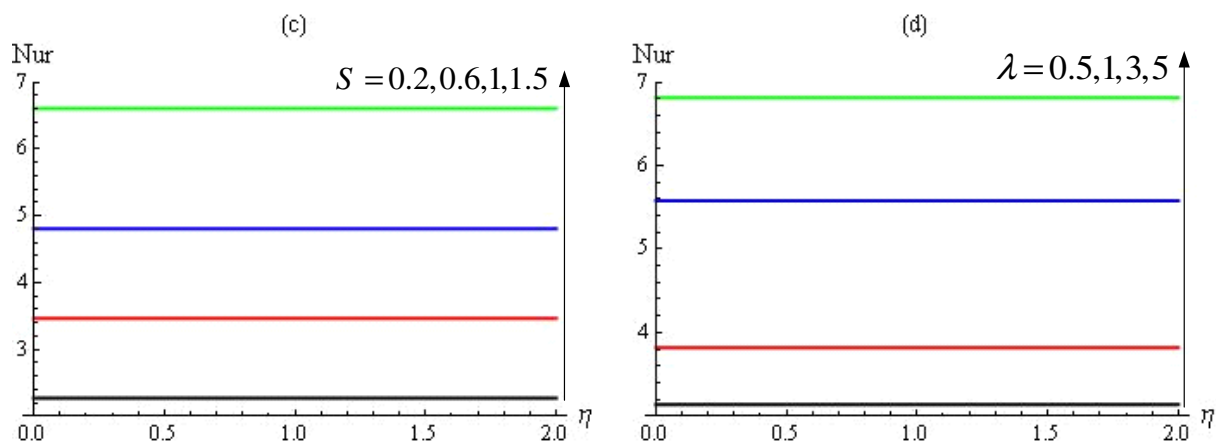


Figure 8. Profiles of the reduced Nusselt number (Nur) as a function of η for different values of the included parameters; in particular for (a) R , (b) M , (c) S and (d) λ .

5. Conclusions

In this research, the hybrid Newtonian incompressible nanofluid flow (Cu-Al₂O₃/water) over a nonlinearly stretching surface was investigated. Then, the governing equations were converted into non-linear ordinary differential equations by applying the proper similarity transformations. Hence, the resulted equations were solved, using the numerical technique Chebyshev pseudo spectral differentiation matrix.

It was deduced that the rising of the mass flux parameter S slows down the velocity and, therefore, decreases the temperature. In addition, the velocity and temperature increases and decreases, respectively, when the stretching parameter λ enlarges. Moreover, the temperature decreases when the values of the temperature parameter m increases. Further, to control the thermal of hybrid nanofluid boundary layer, the radiation parameter can be effectively applied. Furthermore, the solid volume fractions of the included nanoparticle play an important role in the temperature distributions. Finally, the reduced Nusselt number (Nur) increases by raising the values of R , m , S and λ .

Author Contributions: Conceptualization, E.H.A. and I.P.; data curation, E.H.A. and I.P.; formal analysis, E.H.A. and I.P.; funding acquisition, A.V.R.; investigation, E.H.A. and I.P.; methodology, E.H.A.; project administration, A.V.R. and N.C.R.; software, E.H.A.; supervision, E.H.A., N.C.R., A.V.R. and I.P.; validation, E.H.A.; writing—original draft, E.H.A. and I.P.; writing—review and editing, E.H.A., I.P., N.C.R. and A.V.R. All authors have read and agreed to the published version of the manuscript.

Funding: This research received no external funding.

Institutional Review Board Statement: Not applicable.

Informed Consent Statement: Not applicable.

Data Availability Statement: Not applicable.

Conflicts of Interest: The authors declare no conflict of interest.

References

1. Fisher, E.G. *Extrusion of Plastics*, 3rd ed.; Halsted Press: New York, NY, USA, 1976.
2. Tidmore, Z.; Klein, I. *Engineering Principles of Plasticating Extrusion*; Polymer Science and Engineering Series; Van Nostrand: New York, NY, USA, 1970.
3. Crane, L.J. Flow past a stretching plate. *J. Appl. Math. Phys. (ZAMP)* **1970**, *21*, 645–647. [[CrossRef](#)]
4. Choi, S.U.S. Enhancing thermal conductivity of fluids with nanoparticles. In Proceedings of the 1995 ASME International Mechanical Engineering Congress and Exposition, San Francisco, CA, USA, 12–17 November 1995; ASME, FED 231/MD 66; pp. 99–105.
5. Khanafer, K.; Vafai, K.; Lightstone, M.F. Buoyancy-driven heat transfer enhancement in a two-dimensional enclosure utilizing nanofluids. *Int. J. Heat Mass Transf.* **2003**, *46*, 3639–3653. [[CrossRef](#)]

6. Tiwari, R.K.; Das, M.K. Heat transfer augmentation in a two-sided lid-driven differentially heated square cavity utilizing nanofluids. *Int. J. Heat Mass Transf.* **2007**, *50*, 2002–2018. [[CrossRef](#)]
7. Huminic, G.; Huminic, A. Hybrid nanofluids for heat transfer applications—A state-of-the-art review. *Int. J. Heat Mass Transf.* **2018**, *125*, 82–103. [[CrossRef](#)]
8. Aly, E.H.; Pop, I. Merkin and Needham wall jet problem for hybrid nanofluids with thermal energy. *Eur. J. Mech. B/Fluids* **2020**, *83*, 195–204. [[CrossRef](#)]
9. Aly, E.H.; Pop, I. MHD flow and heat transfer near stagnation point over a stretching/shrinking surface with partial slip and viscous dissipation: Hybrid nanofluid versus nanofluid. *Powder Technol.* **2020**, *367*, 192–205. [[CrossRef](#)]
10. Pop, I.; Roşca, N.C.; Roşca, A.V. Additional results for the problem of MHD boundary-layer flow past a stretching/shrinking surface. *Int. J. Numerical Methods Heat Fluid Flow* **2016**, *26*, 2283–2294. [[CrossRef](#)]
11. Roşca, N.C.; Roşca, A.V.; Pop, I. Cross flow and heat transfer past a permeable stretching/shrinking sheet in a hybrid nanofluid. *Int. J. Numerical Methods Heat Fluid Flow* **2021**, *31*, 1295–1319. [[CrossRef](#)]
12. Waini, I.; Ishak, A.; Pop, I. Unsteady flow and heat transfer past a stretching/shrinking sheet in a hybrid nanofluid. *Int. J. Heat Mass Transf.* **2019**, *136*, 288–297. [[CrossRef](#)]
13. Waini, I.; Ishak, A.; Pop, I. Flow and heat transfer along a permeable stretching/shrinking curved surface in a hybrid nanofluid. *Phys. Scr.* **2019**, *94*, 105219. [[CrossRef](#)]
14. Devi, S.U.S.; Devi, S.P.A. Heat transfer enhancement of Cu-Al₂O₃/water hybrid nanofluid flow over a stretching sheet. *J. Niger. Math. Soc.* **2017**, *36*, 419–433.
15. Sarkar, J.; Ghosh, P.; Adil, A. A review on hybrid nanofluids Recent research, development and applications. *Renew. Sustain. Energy Rev.* **2015**, *43*, 164–177. [[CrossRef](#)]
16. Akilu, S.; Baheta, A.T.; Sharma, K.V. Experimental measurements of thermal conductivity and viscosity of ethylene glycol-based hybrid nanofluid with TiO₂-CuO/C inclusions. *J. Mol. Liq.* **2017**, *246*, 396–405. [[CrossRef](#)]
17. Sidik, N.A.C.; Adamu, I.M.; Muhammad, M.J. Preparation methods and thermal performance of hybrid nanofluids. *J. Adv. Res. Mater. Sci.* **2019**, *56*, 1–10.
18. Sundar, L.S.; Sharma, K.V.; Singh, M.K.; Sousa, A. Hybrid nanofluids preparation, thermal properties, heat transfer and friction factor—A review. *Renew. Sustain. Energy Rev.* **2017**, *68*, 185–198. [[CrossRef](#)]
19. Kazemia, M.A.; Jafari, S.S.; Musavi, S.M.; Nejati, M. Analytical solution of convective heat transfer of a quiescent fluid over a nonlinearly stretching surface using Homotopy analysis method. *Results Phys.* **2018**, *10*, 164–172. [[CrossRef](#)]
20. Devi, S.A.; Devi, S.S. Numerical investigation of hydromagnetic hybrid Cu-Al₂O₃/water nanofluid flow over a permeable stretching sheet with suction. *Int. J. Nonlinear Sci. Numer. Simul.* **2016**, *17*, 249–257. [[CrossRef](#)]
21. Cortell, R. Radiation effects for the Blasius and Sakiadis flows with a convective surface boundary condition. *Appl. Math. Comput.* **2008**, *206*, 832–840.
22. Aly, E.H. Dual exact solutions of graphene–water nanofluid flow over stretching/shrinking sheet with suction/injection and heat source/sink: Critical values and regions with stability. *Powder Technol.* **2019**, *342*, 528–544. [[CrossRef](#)]
23. Aly, E.H.; Benlahsen, M.; Guedda, M. Similarity solutions of a MHD boundary–layer flow past a continuous moving surface. *Int. J. Eng. Sci.* **2007**, *45*, 486–503. [[CrossRef](#)]
24. Guedda, G.; Aly, E.H.; Ouahsine, A. Analytical and ChPDM analysis of MHD mixed convection over a vertical flat plate embedded in a porous medium filled with water at 4 °C. *Appl. Math. Model.* **2011**, *35*, 5182–5197. [[CrossRef](#)]
25. Aly, E.H.; Vajravelu, K. Exact and numerical solutions of MHD nano boundary–layer flows over stretching surfaces in a porous medium. *Appl. Math. Comput.* **2014**, *232*, 191–204. [[CrossRef](#)]
26. Aly, E.H.; Sayed, H.M. Magnetohydrodynamic and thermal radiation effects on the boundary-layer flow due to a moving extensible surface with the velocity slip model: A comparative study of four nanofluids. *J. Magn. Magn. Mater.* **2017**, *422*, 440–451. [[CrossRef](#)]
27. Aly, E.H.; Pop, I. Radiation and mixed convection magnetohydrodynamics boundary layer of hybrid Cu-Al₂O₃/water nanofluid flow over a wall jet. *J. Nanofluids* **2020**, *9*, 152–160. [[CrossRef](#)]